LM-04K053
June 9, 2004

Thermophotovoltaic Spectral Control

DM DePoy, PM Fourspring, PF Baldasaro, JF Beausang, EJ Brown, MW Dashiel, KD Rahner, TD Rahmlow, JE Lazo-Wasem, EJ Gratrix and B Wernsman

Thermophotovoltaic Spectral Control

DM DePoy, PM Fourspring, PF Baldasaro, JF Beausang, EJ Brown, MW Dashiel, KD Rahner
Lockheed Martin Corporation, Schenectady, NY

TD Rahmlow, JE Lazo-Wasem, EJ Gratrix
Rugate Technologies, Inc., Oxford, CT

B Wernsman
Bechtel Bettis, Inc., West Mifflin, PA

Abstract

Spectral control is a key technology for thermophotovoltaic (TPV) direct energy conversion systems because only a fraction (typically less than 25%) of the incident thermal radiation has energy exceeding the diode bandgap energy, E_g, and can thus be converted to electricity. The goal for TPV spectral control in most applications is twofold:

1. Maximize TPV efficiency by minimizing transfer of low energy, below bandgap photons from the radiator to the TPV diode.
2. Maximize TPV surface power density by maximizing transfer of high energy, above bandgap photons from the radiator to the TPV diode.

TPV spectral control options include: front surface filters (e.g. interference filters, plasma filters, interference/plasma tandem filters, and frequency selective surfaces), back surface reflectors, and wavelength selective radiators. System analysis shows that spectral performance dominates diode performance in any practical TPV system, and that low bandgap diodes enable both higher efficiency and power density when spectral control limitations are considered. Lockheed Martin has focused its efforts on front surface tandem filters which have achieved spectral efficiencies of ~83% for E_g = 0.52 eV and ~76% for E_g = 0.60 eV for a 950 ^oC radiator temperature.

Introduction

There is currently a resurgence of development activity in the area of thermophotovoltaic (TPV) energy conversion that has been driven by advancements in III-V semiconductor technology and the potential use of TPV in a wide range of applications. TPV systems have several performance advantages over other energy conversion technologies, including: 1) the wide range of available fuel sources, 2) the absence of moving parts which provides low noise and high reliability, and 3) the near term potential to achieve high system efficiency (> 20%).

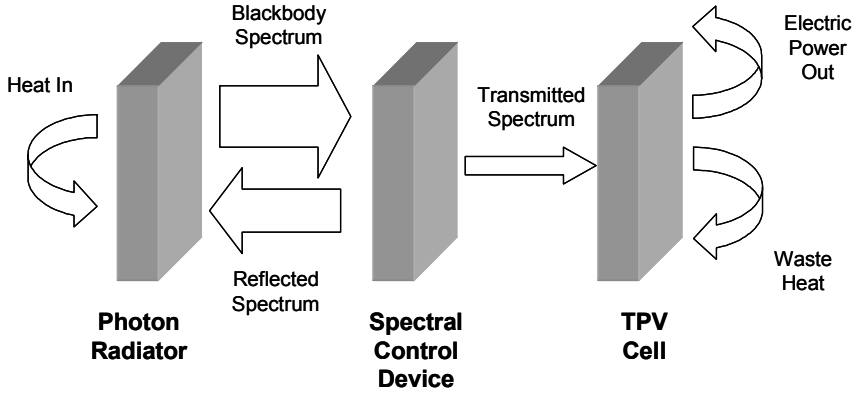

Figure 1: Schematic of TPV conversion components

The basic components of a TPV conversion system are described in Figure 1 and include: a photon radiator, a spectral control device, and a TPV diode with a bandgap (E_g). The TPV process can be conceptualized as the selective conversion of photons from the radiator which have energies greater than the diode bandgap ($E > E_g$). The conversion process incorporates a spectral control device to minimize parasitic absorption of photons of unusable energy ($E < E_g$). In essence, the spectral control device serves as a photon recuperator to minimize the heat required to keep the radiator at temperature. The goal for TPV spectral control in most applications is twofold:

1. Maximize TPV efficiency ($\eta_{TPV} = \eta_{diode} \cdot \eta_{spectral} \cdot \eta_{module}$) by minimizing transfer of low energy, below bandgap photons from the radiator to the TPV diode.

2. Maximize TPV surface power density by maximizing transmission ($T_{>Eg}$) of high energy, above bandgap photons from the radiator to the TPV diode

In practice, TPV spectral control may not be separable into independent components as suggested in Figure 1. For example, the radiator may provide spectral control by tailoring the emission spectrum; or the diode may provide spectral control if it is designed to be transparent to below-bandgap energy and a reflective surface is placed on the back side of the diode to reflect the below-bandgap energy back to the radiator.

TPV spectral control technologies can be divided into two categories according to the temperature at which they operate: cold side or hot side. Cold side TPV spectral control technologies are coupled to the TPV system heat sink, are kept at a low temperature (typically 20 – 50 ^{o}C), and provide spectral control by reflecting low energy (long wavelength) photons back to the radiating surface. Cold side spectral control technologies include front surface filters and back surface reflectors (BSR). Examples of front surface filters that have been considered for use in TPV applications include: photonic bandgap filters with periodicity in one dimension (e.g. interference filters), two dimensions (e.g. frequency selective surfaces), and three dimensions; plasma filters; and various combinations (e.g. interference/plasma tandem filter). Hot side TPV spectral control technologies are coupled to the heat source (at approximately the same temperature as the heat source) and provide spectral control by suppressing emission of low energy photons from the radiating surface. Hot side spectral control can be accomplished by texturing the surface of the radiator, applying coatings or filters to the surface of the radiator, using bulk radiator materials with selective emission characteristics (e.g. rare earth oxides), or utilizing a three dimensional photonic bandgap (PBG) structure. TPV spectral control technologies are summarized in Table 1.

Table 1: TPV Spectral Control Technologies

Radiator	• Selective Radiator • Textured Radiator • Filtered Radiator • 3D Photonic Bandgap Radiator
Gap	↑ **Hot Side** ↓ **Cold Side**
Front Surface	• Plasma Filter • 1-D Photonic Bandgap Filters (Interference Filter) • 2-D Photonic Bandgap Filters (Frequency Selective Surface (FSS) Filter) • 3-D Photonic Bandgap Filter • Tandem Filters (Combination of Interference Filter and Plasma Filter)
TPV Cell	
Back Surface	• Back Surface Reflector

A summary of the key technical results from our TPV spectral control research and development efforts on front surface tandem filters, frequency selective surfaces, and back surface reflectors is presented below following a discussion of the fundamental challenges associated with TPV spectral control, identification of TPV spectral control figures of merit, the impact of cavity photonics on TPV spectral control, and the importance of TPV diode bandgap on TPV spectral performance. A literature review on the use of wavelength selective radiators for TPV spectral control is also presented.

Discussion

TPV Spectral Control Challenges

The unique spectral and angular attributes of blackbody radiation have a significant impact on spectral control device design and overall TPV system efficiency. The wavelength (λ) and radiator temperature (T_h) dependence of radiation from a blackbody is defined by Planck's spectral distribution of emissive power:

$$N(\lambda, T_h) = \frac{2\pi hc^2}{\lambda^5} \cdot \left[\exp\left(\frac{hc}{k_B \lambda T_h} \right) - 1 \right]^{-1} \qquad (1)$$

where h is Planck's constant, k_B is Boltzman's constant, and c is the speed of light. Figure 2 compares the spectral distribution of the energy flux for solar radiation (6035 ^oC) incident at the Earth's surface to a blackbody source at 950 ^oC.

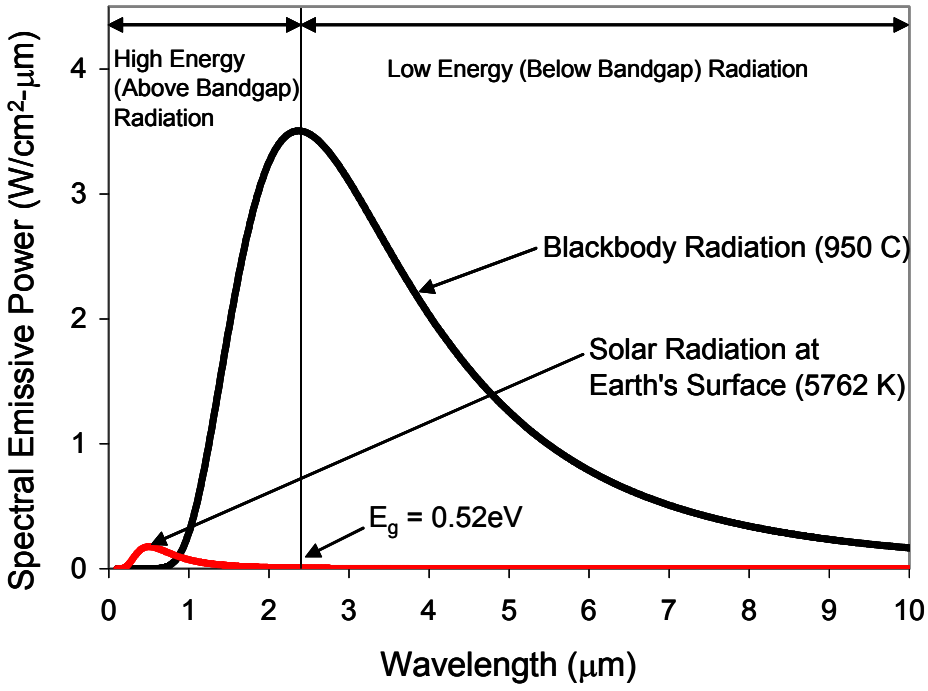

Figure 2: Comparison of solar vs TPV spectrum

The lower temperature TPV blackbody source shows a significantly longer average wavelength content (i.e. lower energy) vs. the solar source. In addition, the blackbody spectrum for 950 ^oC radiator temperature covers a much broader spectral range compared to the solar spectrum. 95% of the radiated power from a 950 ^oC blackbody is contained in the wavelength range from 1 μm to 10 μm

compared to the wavelength range from 0.2 μm to 2 μm for the solar spectrum. The large spectral range of a TPV blackbody radiator necessitates a very wide (~2 μm - 10 μm) reflection bandwidth for cold side spectral control technologies and/or a very wide suppressed emission bandwidth for hot side spectral control technologies. This requirement imposes significant constraints on spectral control design and performance from a materials selection viewpoint. For example, front surface filter materials must have very low absorption (extinction coefficient < 0.001) over the spectral range of 1 μm to greater than 10 μm in order to achieve high transmission of high energy, above bandgap photons and high reflection of low energy, below bandgap photons.

Another key issue with TPV spectral control is the low fraction of usable energy ($E > E_g$) in the radiated blackbody spectrum. The fraction of usable above-bandgap energy as a function of diode bandgap is shown in Figure 3 for T_h = 950 °C. As shown in Figure 3, the fraction of usable above-bandgap energy for E_g = 0.52 eV is only about 28%. The remaining 72% of the incident radiation cannot be converted to electricity, and, therefore, must be recuperated by the spectral control device in order to maximize TPV efficiency. The low fraction of usable above-bandgap energy amplifies the effect of parasitic photon absorption.

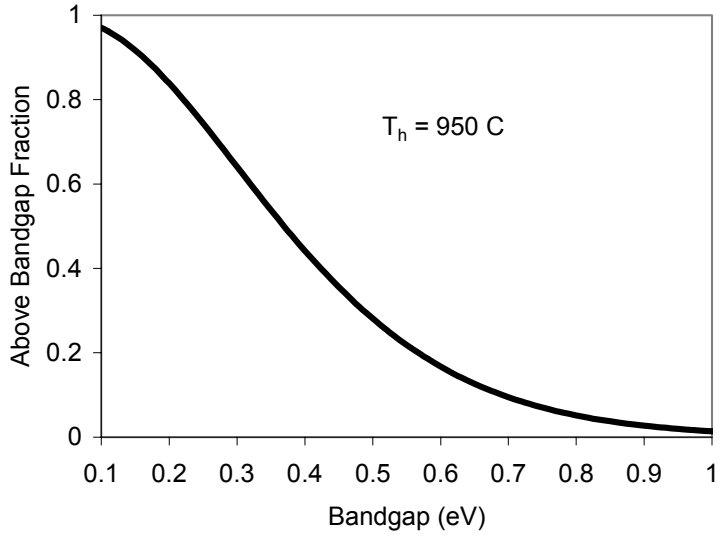

Figure 3: Usable ($E>E_g$) energy fraction vs E_g for T_h = 950 °C

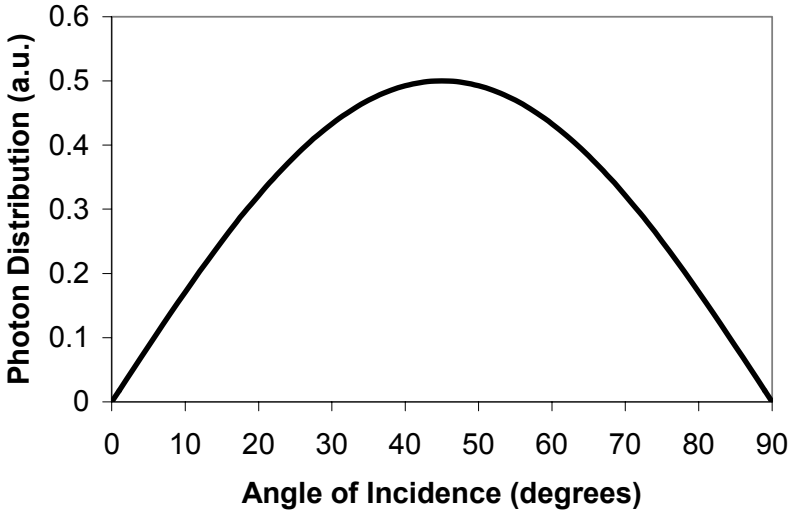

Figure 4: Photon distribution as a function of angle of incidence

It is important to note that photons are incident on the diode or filter (if applicable) surface from all angles of incidence (AOI). The angular dispersion of photons incident on the TPV cold side from a Lambertian TPV radiator surface in an infinite flat plate geometry follows a $\sin\theta \cdot \cos\theta$ dependence [1] where θ is angle of incidence. As shown in Figure 4, this dependence has a peak value at 45 degrees, compared to the near-normal solar spectrum (the result of the large Earth-sun separation).

The large angular dispersion of the Blackbody TPV source complicates spectral control design and performance in several ways:

- Interference-based filters depend on the optical path length of filter layers, which in turn depends on the angle of photon incidence. The large photon angular dispersion (0^o- 90^o) leads to a performance compromise for a fixed filter design.

- The high angular dispersion of incident photons, together with non-specular reflections, lead to the potential for optical frustration [2], (i.e. trapping and multiple internal reflections within the high refraction index layers of the diode/filter). Frustration can be a major parasitic absorption loss process even for near-zero absorption materials because of the long path lengths.

- At incidence angles greater than 70^o (which represent ~ 12% of the TPV blackbody photon population), the reflection probability increases as predicted from Fresnel's laws ($R \propto \sin^2\theta$). High angle reflection limits the transmission of above-bandgap energy and lowers TPV surface power density.

Figures of Merit for TPV Spectral Control

The performance of any spectral control method can be characterized by two key figures of merit: spectral efficiency ($\eta_{spectral}$) and integrated above bandgap transmission ($T_{>Eg}$). These figures of merit capture the spectral control performance that relates to the conversion efficiency and power density of a TPV system. Specifically, TPV efficiency is proportional to spectral efficiency and TPV surface power density (W/cm^2) is proportional to integrated above bandgap transmission. Spectral efficiency, Eq. (2), is defined as the ratio of the integrated above bandgap power absorbed in the TPV cell to the total power absorbed. Integrated above bandgap transmission is the ratio of the integrated above bandgap power absorbed by the TPV cell to the above bandgap power radiated from a perfect ($\varepsilon(\lambda,\theta)=1$) blackbody, Eq. (3):

$$\eta_{spectral} = \frac{\int_0^{\frac{\pi}{2}}\int_0^{\lambda_g} \varepsilon_{eff}(\lambda,\theta,T_h)\frac{T(\lambda,\theta)}{1-R(\lambda,\theta)}N(\lambda,T_h)\sin\theta\cos\theta d\lambda d\theta}{\int_0^{\frac{\pi}{2}}\int_0^{\infty} \varepsilon_{eff}(\lambda,\theta,T_h)N(\lambda,T_h)\sin\theta\cos\theta d\lambda d\theta} \quad (2)$$

$$T_{>Eg} = \frac{\int_0^{\frac{\pi}{2}}\int_0^{\lambda_g} \varepsilon_{eff}(\lambda,\theta,T_h)\frac{T(\lambda,\theta)}{1-R(\lambda,\theta)}N(\lambda,T_h)\sin\theta\cos\theta d\lambda d\theta}{\int_0^{\frac{\pi}{2}}\int_0^{\lambda_g} N(\lambda,T_h)\sin\theta\cos\theta d\lambda d\theta} \quad (3)$$

Where

- $R(\lambda,\theta)$ is the reflectance as a function of wavelength and angle of incidence of the cold side which can be:
  - a front surface filter on a TPV diode (with or without a BSR)

- a TPV diode (with or without a BSR) with an antireflection coating
- a bare TPV diode (with or without a BSR)

- $T(\lambda,\theta)$ is the transmittance as a function of wavelength and angle of incidence of the cold side as a function of wavelength and angle of incidence and is equal to 1- $R(\lambda,\theta)$ for spectral control technologies that do not utilize a front surface filter
- λ_g is the wavelength corresponding to the band gap (E_g) of the TPV diode
- $\varepsilon_{eff}(\lambda,\theta,T_h)$ is the effective emissivity, which for infinite, parallel plates is defined:

$$\varepsilon_{eff}(\lambda,\theta,T_h) = \frac{1}{\frac{1}{\varepsilon_{rad}(\lambda,\theta,T_h)} + \frac{1}{1-R(\lambda,\theta)} - 1} \tag{4}$$

- $\varepsilon_{rad}(\lambda,\theta,T_h)$ is the radiator emissivity as a function of wavelength, angle of emission and temperature

Note that $\varepsilon_{eff}(\lambda, \theta, T_h)$ simplifies to1 - $R(\lambda,\theta)$ for the ideal case of a blackbody radiator ($\varepsilon_{rad} = 1$), and that the $T(\lambda,\theta)$ /(1- $R(\lambda,\theta)$) term in Eq. (2) and (3) accounts for parasitic absorption of above bandgap photons in a front surface filter (if applicable). It is also useful to define the integrated below bandgap effective emissivity, $\varepsilon_{<Eg,eff}$, as follows:

$$\varepsilon_{<Eg,eff} = \frac{\int_0^{\frac{\pi}{2}} \int_{\lambda_g}^{\infty} \varepsilon_{eff}(\lambda,\theta,T_h) N(\lambda,T_h) \sin\theta\cos\theta d\lambda d\theta}{\int_0^{\frac{\pi}{2}} \int_{\lambda_g}^{\infty} N(\lambda,T_h) \sin\theta\cos\theta d\lambda d\theta} \tag{5}$$

These figures of merit for TPV spectral control performance, account for the spectral weighting of radiant energy, the wavelength and angular dependent optical properties of components, and nonlinear cavity effects due to multiple bounces of photons between the radiator and the TPV cold side. In addition, these figures of merit are valid for any spectral control method or combination of methods and have been shown to correlate with the measured in-cavity efficiency and power density of a combined TPV cell and spectral control configuration [3,4].

Examination of Eq. (2) indicates that high spectral efficiency requires a spectral control technology with very low below bandgap effective emissivity, high integrated above bandgap transmission , and low parasitic absorption of above bandgap photons in the filter (if applicable). Figure 5 shows the relationship between spectral efficiency and integrated below bandgap effective emissivity for T_h=950 ^oC, integrated above bandgap transmission = 85%, 0% above bandgap parasitic filter absorption, and TPV diode bandgaps of 0.4 eV, 0.5 eV, 0.6 eV, and 0.7 eV. As shown in Figure 5, spectral efficiency is a strong function of integrated below bandgap emissivity and TPV diode bandgap. Higher integrated below bandgap effective emissivity results in higher parasitic absorption and lower spectral efficiency. Spectral efficiency is higher for lower bandgap TPV devices because the above bandgap fraction is higher (Figure 3). In order to achieve spectral efficiencies of 85%, integrated below bandgap emissivity must be less than 12%, 6%, 3%, and 1.6% for 0.4 eV, 0.5 eV, 0.6 eV, and 0.7 eV diode bandgap respectively.

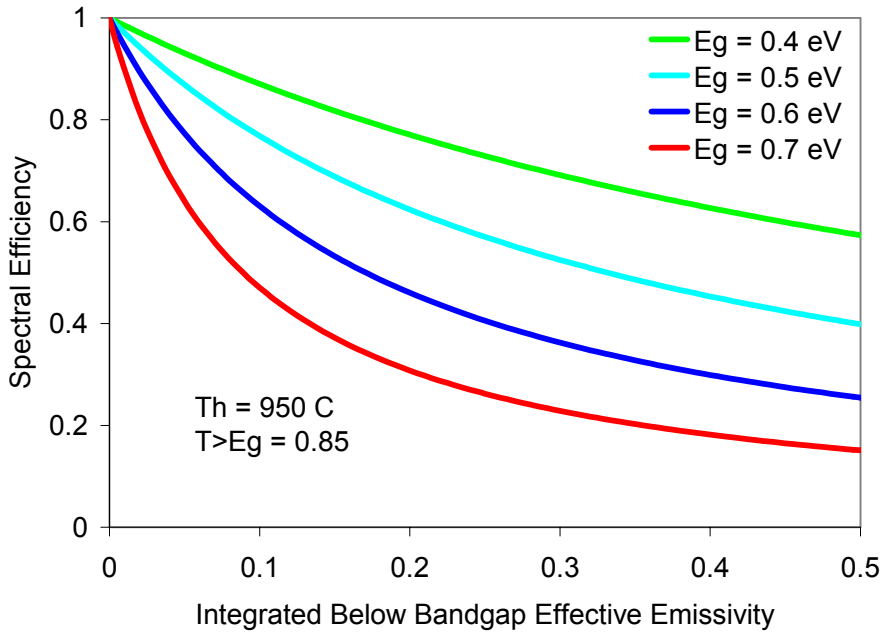

Figure 5: Spectral Efficiency versus Integrated Below Bandgap Effective Emissivity

Photonic Cavity Issues

TPV system design introduces unique photonic issues, which affect efficiency and power density. For example, a TPV converter necessarily involves some sort of cavity [5]. From a photonic viewpoint, the key TPV cavity attributes are:

1. parasitic absorption at inactive cold side areas (e.g. grids, busbars, and gaps between diodes)
2. angular and polarization dependent radiator emissivity (i.e., non-Lambertian),
3. angular and polarization dependent front surface filter reflectivity
4. finite separation between radiator and diode which alters the angular dispersion
5. cavity edge leakage or sidewall absorption

These non-ideal cavity attributes complicate the photon recuperation. In general, advanced numerical techniques such as Monte Carlo and photon ray tracing are needed to quantify the impact of these processes on TPV performance [2,5].

The impact of parasitic absorption in inactive cold side areas on TPV efficiency can be quantified via a module efficiency factor, η_{module}. η_{module} is directly proportional to TPV efficiency and is defined as the total photonic energy absorbed in active diode area divided by total photonic energy absorbed. Figure 6 shows the results of a simplified cavity analysis that examines the impact of inactive area and its reflectivity (assumed to be constant with wavelength and AOI) on η_{module}. This analysis is based on the following assumptions:

- $\varepsilon_{rad}(\lambda,\theta) = 0.9$
- use of a front surface filter with
  - integrated above bandgap filter reflection = 15%
  - integrated above bandgap filter parasitic absorption = 2%
- $T_h = 950\ ^oC$
- $E_g = 0.5$ eV

As shown in Figure 6, both the fraction of active area and the reflectivity of inactive area ($R_{inactive}$) have a strong influence on module efficiency; for example, 85% active area and 90% inactive area

reflectivity results in η_{module}~0.9. Figure 7 shows η_{module} versus inactive area reflectivity for TPV diode bandgaps of 0.4, 0.5, 0.6, and 0.7 eV assuming 85% active area. As shown in Figure 7, η_{module} is also a strong function of the TPV diode bandgap with higher diode bandgaps resulting in lower module efficiency. This result is expected since the diode bandgap plays a major role in determining the total photonic energy absorbed, but does not impact parasitic absorption in the inactive area. The large variation in module efficiency shown in Figure 6 and Figure 7 indicate the importance of including cavity photonic issues when estimating TPV system performance.

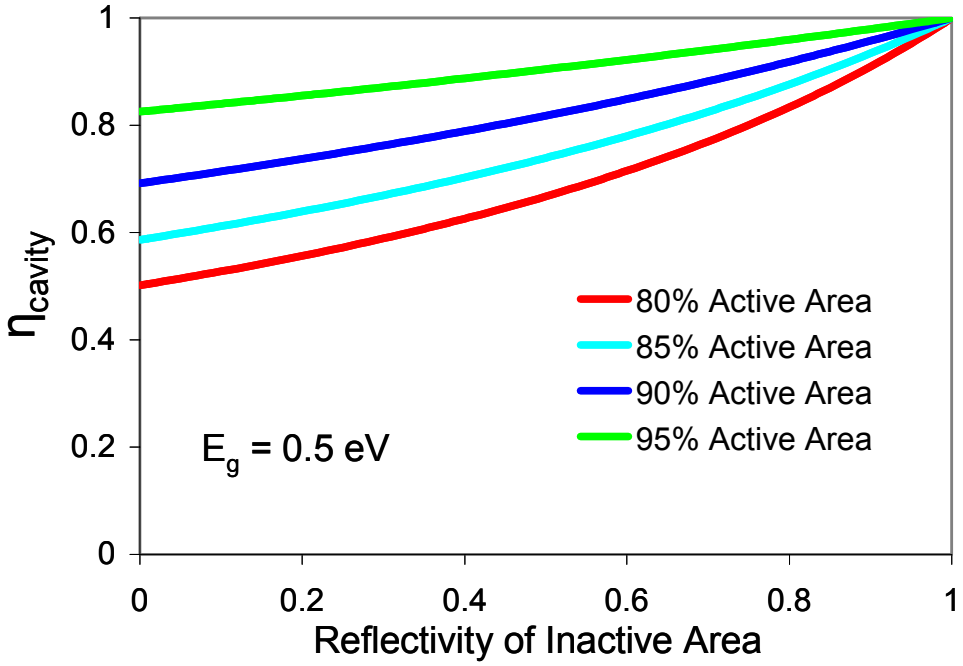

Figure 6: Module Efficiency versus Inactive Area Reflectivity and Active Area Fraction

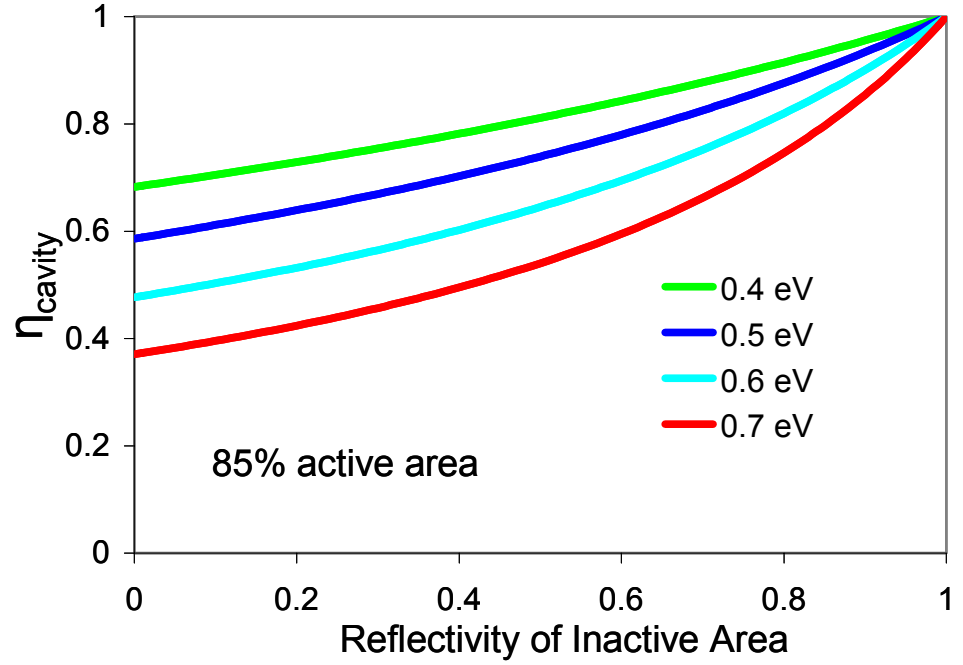

Figure 7: Module Efficiency versus Inactive Area Reflectivity and Diode Bandgap

TPV Efficiency and Power Density versus Diode Bandgap

Figure 8 presents calculations of TPV efficiency, η_{TPV}, and output power density, P_{out} (W/cm^2), as a function of diode bandgap and integrated below bandgap effective emissivity. Using the spectral efficiency and module efficiency defined above, TPV efficiency is calculated from:

$$\eta_{TPV} = P_{out}/q_{total} = \eta_{diode} \cdot \eta_{spectral} \cdot \eta_{module} \quad (6)$$

$$\eta_{diode} = QE \cdot F_o \cdot q_0 V_{oc} / E_g \cdot FF \quad (7)$$

where:

- q_{total} is the total heat flux absorbed (W/cm^2)
- η_{diode} is the TPV diode efficiency
- QE is the photon weighted internal quantum efficiency
- F_o is the photon over excitation efficiency
- $q_0 V_{oc} / E_g$ is the open circuit voltage efficiency (q_0 is the charge of an electron)
- FF is the power usage efficiency or fill factor

The following assumptions were made in this parameter study:

- integrated above bandgap transmission = 76% (consistent with 90% above bandgap radiator emissivity, 15% above bandgap filter reflectivity and 2% above bandgap filter absorption)
- radiator temperature = 950 ^oC
- diode temperature = 50 ^oC
- QE = 95%
- FF = 0.95 x $FF_{Rs=0}$ = 95% of the zero series resistance fill factor
- 10% inactive area with reflectivity as indicated in Figure 8

These assumptions are consistent with the performance of state-of-the-art TPV cells and filters. The following correlation for TPV diode dark current density versus diode bandgap and diode temperature was used in this parameter study:

$$J_o \text{ (A/cm}^2\text{)} = 1.583 \times 10^{-5} \cdot \exp(2.912\, E_g) \cdot (T_{diode})^3 \cdot \exp(-E_g / k_B\, T_{diode}) \quad (8)$$

Equation 8 is based on a correlation from Wanlass [6], scaled to be consistent with PC-1D analysis of the projected performance (based on engineering limits) of 0.52 eV InGaAsSb TPV diodes [7] and 0.60 eV InGaAs diodes. The following assumptions were used in the PC-1D analyses:

- diode thickness = 2.8 μm
- front and back surface recombination velocity = 10 cm/sec
- Shockley Reed Hall recombination lifetime = 3μs
- Auger recombination coefficient, C = 10^{-28} cm^6/sec
- Radiative recombination and photon recycling modeled using an effective radiative recombination coefficient: $B_{eff} = B/\varphi = 2.86 \times 10^{-12}$, where B is calculated using the vanRoosbroek-Shockley relationship and the photon recycling factor, φ, is calculated according to Asbeck [8] assuming a 100% reflecting back surface.

Figure 8 shows that even low levels of integrated below bandgap effective emissivity have a significant effect on TPV efficiency and on the location of the optimum (peak efficiency) diode bandgap. Note that efficiency is a weak function of diode bandgap near the peak efficiency whereas power density is a strong function of diode bandgap in this same range.

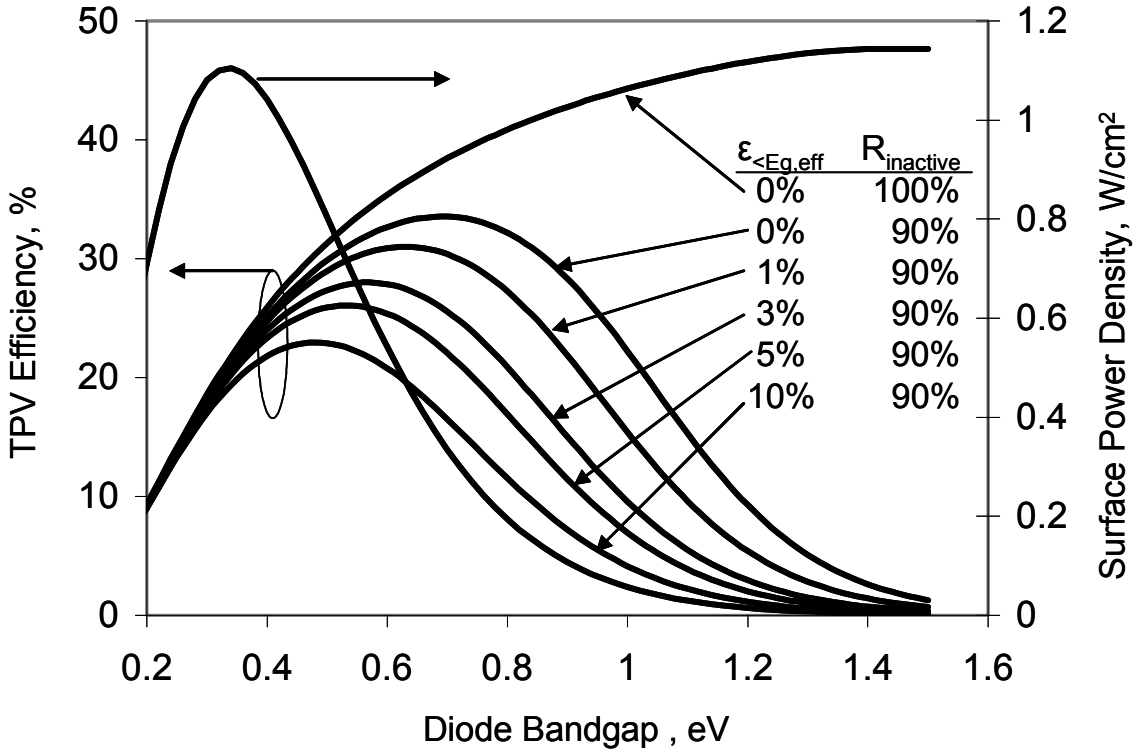

Figure 8: TPV Efficiency and Power Density versus Diode Bandgap

The importance of bandgap on efficiency enters via the determination of the fraction of usable energy (for a given radiator temperature), which subsequently affects spectral efficiency (Figure 5). The strong dependence of TPV efficiency on spectral performance for diode bandgaps greater than ~0.4 eV is a result of the relatively low fraction of above bandgap photons. It is a key conclusion that lower bandgap diodes can enable both higher power density and higher efficiency when spectral control limitations are included. In addition, spectral control performance plays a major role in defining the diode bandgap that provides the peak TPV efficiency. In effect, spectral performance (recuperation) in TPV systems is dominant over diode performance (conversion), and, for a desired radiator temperature, determines the optimum diode bandgap.

Results

Front Surface Tandem Filters

The highest TPV spectral performance to date has been achieved using a front surface tandem filter [9,10,11]. As shown in Figure 9, the tandem filter concept is the combination of a plasma filter with an interference filter [12,13,14]. The interference filter provides high transmission of above bandgap photons, high reflection of below bandgap photons from the bandgap wavelength to ~ 6 μm, and a sharp transition from high transmission to high reflection at or near the bandgap wavelength. The plasma filter provides low absorption for above bandgap photons and high reflection for below bandgap photons with wavelength greater than ~6 μm. Figure 9 also illustrates the performance of the tandem filter concept by showing the spectral response of the interference filter, the plasma filter, and the combination of the two into a tandem filter.

The plasma filter consists of a heavily doped (~$5x10^{19}$ cm^{-3}) n-type (doped with Te) layer of $InP_{.75}As_{.25}$ epitaxially grown using OMVPE onto a double side polished InP substrate [15,16]. This plasma filter has a plasma wavelength of 4.5 μm to 5 μm. Essentially, the plasma filter acts like a dielectric in the short wavelength above bandgap spectral region and acts like a metal in the long wavelength spectral region.

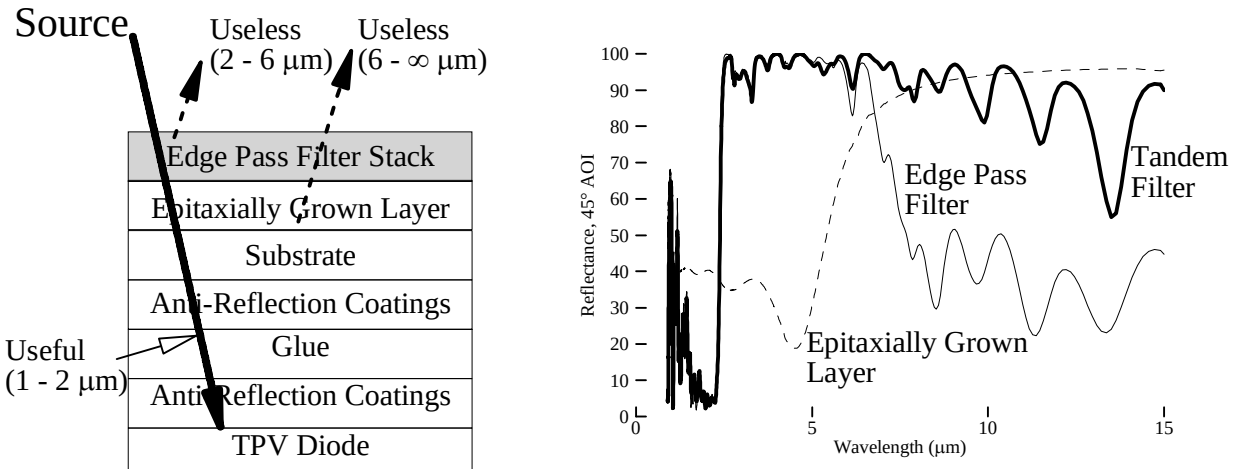

Figure 9: Tandem Filter Concept

The interference filter consists of a multilayer stack of dielectric materials. Sb_2Se_3 (n~3.4) is used as the high index of refraction material and YF_3 (n~1.5) is used as the low index of refraction material. The development of Sb_2Se_3 as a high index of refraction interference filter material is a key program achievement that has enabled high TPV spectral performance. Sb_2Se_3 provides a high index of refraction (~3.4) and a very low extinction coefficient (<0.0001) *across the entire spectral range* (from 0.85 μm to greater than 30 μm).

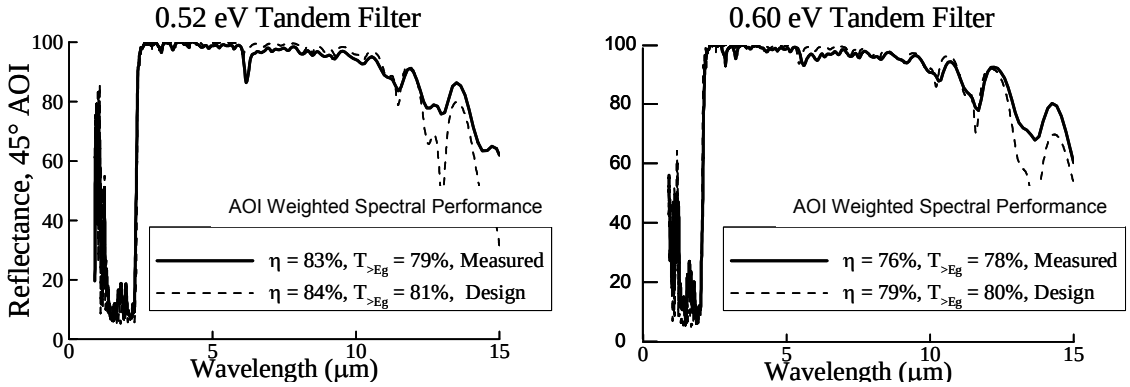

Assumptions: T_h = 950°C, $\varepsilon_{radiator}$ = 1.0 (all λ)

Figure 10: Measured and Predicted Tandem Filter Performance

Figure 10 shows the measured and predicted reflection (45 AOI) versus wavelength of tandem filters fabricated for 0.52 eV and 0.60 eV TPV diodes. The measured results are in excellent agreement with predictions made using OptiLayer™ thin film design software. Specifically, the measured results show very high reflectivity in the below bandgap region, minimal edge shift with angle of incidence, and sharp transition at the bandgap wavelength. Sb_2Se_3/YF_3 tandem filters represent the highest spectral performance achieved to date for TPV spectral control. Specifically, tandem filters have achieved spectral efficiencies of ~83% for E_g = 0.52 eV and ~76% for E_g = 0.60 eV for a 950 ^oC radiator temperature. Table 2 provides a summary of recent in-cavity TPV efficiency measurements for two TPV diode material systems using tandem filters or BSR spectral control at various operating conditions (radiator and diode temperature).

Table 2: Summary of Recent In-Cavity TPV Efficiency Measurements

Diode Material System	Bandgap (eV)	Spectral Control Method	$T_{radiator}$ (^oC)	T_{diode} (^oC)	η_{TPV} (%)	Reference
InGaAs	0.6	Tandem Filter	871	24	19.4	4
			955	24	22.3	
			1039	25	23.6	
			955	52	20.0	
		BSR	955	26	18.6	
			956	54	16.9	
InGaAsSb	0.52	Tandem Filter	950	27	19.5	7
			950	54	17.0	

Frequency Selective Surfaces

Another type of front surface filter is a frequency selective surface (FSS). An FSS is a 2 dimensional periodic array of electromagnetic scattering elements (metal holes or patches) with wavelength selective spectral properties that depend on the size, shape, and spacing of the elements [17]. It has been proposed that an FSS with sub-micron feature size would be a suitable filter for thermal radiation (1-10 μm) in a TPV application [18,19,20]. Our program has been considering FSS as an alternate filter technology; however, as described below, spectral performance of both fabricated and modeled FSS structures is significantly lower than the tandem filter.

FSSs selectively reflect and transmit incident radiation depending on the superposition of the incident field and the scattered field that result from induced currents in the metallic FSS. The induced currents are determined by the geometry of the FSS and can be represented by a resonant circuit of inductive, capacitive, and resistive elements [17]. The resistance is due to the finite conductivity of the metal structure, and results in ohmic losses that are measured as absorption in the FSS structure. An FSS modeled as a perfect electrical conductor does not show any absorption. This absorption mechanism is thus intrinsic to FSS operation given the finite conductivity of the metal [21,22,23] and is particularly detrimental to TPV filter performance because the peak absorption occurs at or near the peak in filter transmission. Physically, the peak absorption is a maximum at the filter resonance because the induced currents reach peak values and the maximum fraction of the FSS metal (i.e. both sides of the filter) participates in the resonant behavior [22].

Table 3: Comparison of Tandem and FSS Filter Performance [a]

Filter Technology	Filter efficiency η_{filter}	Integrated above-bandgap transmission $T_{E>Eg}$	Integrated above-bandgap absoprtion $A_{E>Eg}$	Integrated above-bandgap reflectivity $R_{E>Eg}$	Integrated below-bandgap reflectivity $R_{E<Eg}$
TPV Filter Goal	**85-90 %**	**85%**	**3%**	**15%**	**97%**
Tandem filter[b] (measured)	**80%**	**80%**	**3%**	**18%**	**94%**
Tandem filter[c] (calculated)	**85%**	**84%**	**3%**	**13%**	**96%**
Ring-aperture FSS[e] (measured)	**~48%**	**~45%**	**~12%**	**~43%**	**~80%**
Ring-aperture FSS[d] (calculated)	**~50%**	**~40%**	**~14%**	**~46%**	**~85%**
Al Wire-mesh FSS[d] (calculated)	**~55%**	**~80%**	**~7%**	**~13%**	**~68%**
Wire-mesh FSS[e] (measured)	**~45%**	**~71%**	**~5%**	**~24%**	**~67%**
Wire-mesh FSS[d] w/ Tandem Filter[c] (estimated)	**~75%**	**~66%**	**~5%**	**~29%**	**~93%**

a) Parameters calculated for optimal diode bandgap (0.45-0.55eV) and radiator temperature T_{rad} = 950°C and perfect blackbody radiator (ε=1)
b) Angle-of-incidence weighted
c) 45° Angle-of-incidence
d) 0° Angle-of-incidence
e) 11° Angle-of-incidence

Table 3 provides a summary of measured and predicted spectral control performance calculations for several FSS filters. In general, all FSSs fabricated and/or modeled by our program to date exhibit low above-bandgap transmission, high absorption in the filter pass band, and significant degradation in spectral performance for off-design angles of incidence (polar and azimuthal). One exception to this is the wire mesh FSS geometry, which had low below-bandgap reflectivity. The origin of the pass-band absorption is attributed to ohmic losses in the FSS metallization, and is believed to be inherent—even in a perfectly fabricated structure—as it is the result of the induced currents in the finite conductivity FSS metal. If it is assumed that FSS filters could be optimized for isotropic infrared radiation and if the above-bandgap reflectivity could be reduced, then the significant absorption in the pass band would still be a fundamental obstacle to incorporating FSS into high-efficiency high-power density TPV spectral control. It is thus concluded that FSS with conventional metallizations (those other than superconducting materials, which were not considered) do not satisfy the strict requirements for high spectral efficiency and high above-bandgap transmission as compared to current tandem filter technology.

Back Surface Reflectors

Another TPV spectral control option is a back surface reflector [24,25,26]. As shown in Figure 11 the above bandgap energy is absorbed in the diode layers while the below bandgap energy passes through the diode and is reflected from the back surface reflector back through the device and returned to the radiator. The measured spectral performance of a 0.60 eV InGaAs monolithically integrated module (MIM) with a back surface reflector and a single layer Si_3N_4 antireflection coating is shown in Figure 11 for both unprocessed and processed (i.e. addition of grid fingers and trenches needed for the MIM concept) material. These results represent the highest spectral performance our program has achieved to date using the BSR concept. This BSR achieved 55% spectral efficiency with 84% integrated above bandgap transmission assuming a 950 °C blackbody radiator. As shown in Table 2, 16.9% in-cavity TPV efficiency has been measured using 0.6 eV InGaAs MIM with a BSR ($T_{radiator}$ = 956 °C, T_{diode} = 54 °C) [4].

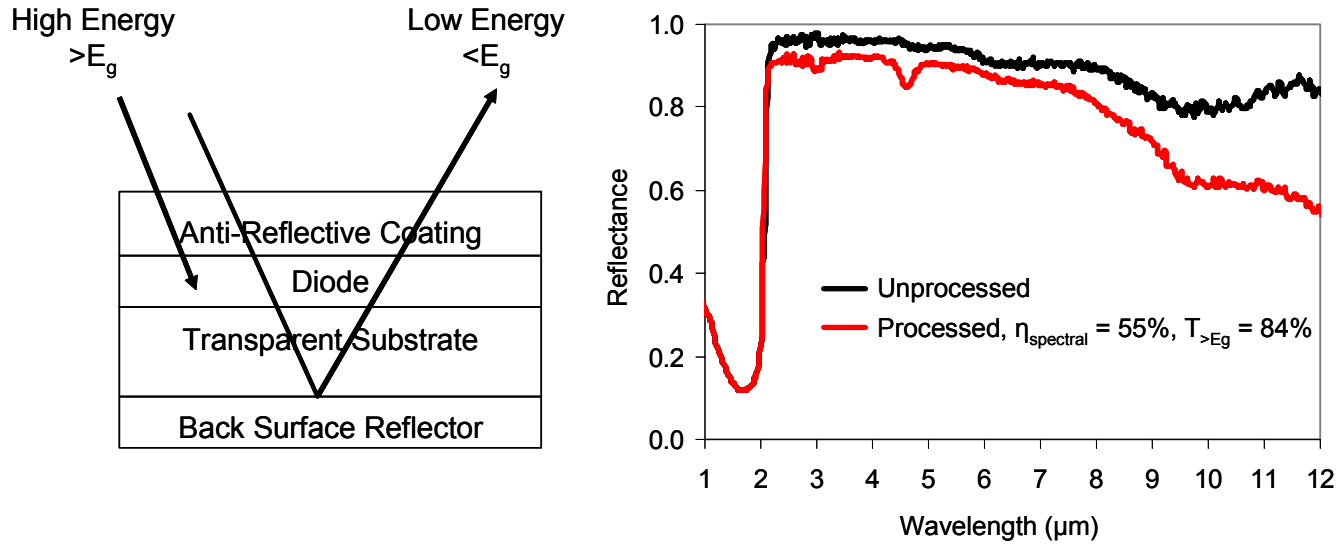

Figure 11: Measured Reflection versus Wavelength for BSR before and after MIM processing

Spectral performance of the BSR concept is primarily limited by free carrier absorption in the TPV diode layers. Free carrier absorption in the diode layers or diode substrate reduces long wavelength reflectivity. Therefore, low diode layer doping and a very low doped semi-insulating substrate (e.g. InP) should be used to maximize BSR spectral performance. Alternatively, in some diode concepts, substrate thinning or removal could be performed to mitigate the absorption caused by a conducting substrate. In most diode architectures, free carrier absorption causes a trade-off between diode and spectral performance (i.e. higher doping in some diode layers improves diode performance at the

expense of BSR spectral performance). In addition, as shown in Figure 11, TPV device processing causes light scattering and trapping which results in a further reduction of below bandgap reflectance.

The BSR spectral control option has the advantage of being less complicated than a tandem filter (2 layer dielectric/metal deposited on back of TPV diode compared to >50 layers for tandem filters) and it provides higher integrated above bandgap transmission (84% for BSR compared to about 80% for tandem filters). However, current BSR spectral efficiency is significantly lower than current tandem filter spectral efficiency (~55% for BSR compared to ~75% for tandem filters for 950 C blackbody radiator with 0.60 eV diode bandgap). Diode design and fabrication experience to date indicates that there is little room for improvement of the BSR spectral performance without significantly impacting diode performance.

Wavelength Selective Radiators

Numerous investigators have pursued development of hot side TPV spectral control technologies which include: selective, textured, filtered, or photonic crystal radiators [27-36]. Selective radiators (e.g. rare earth oxides) represent the use of bulk materials with intrinsic spectral emittance properties at the required temperature of operation. Surface modification can be used for textured TPV radiators to increase the short wavelength ($E>E_g$) emissivity of a base material with low long wavelength ($E<E_g$) emissivity (e.g. tungsten). A filtered radiator enhances the intrinsic, spectral emittance by applying thin layers on the bulk radiator material. A 3D photonic crystal radiator has been postulated for use as either an engineered bulk radiator material or a filter on a bulk radiator material. As a filter the 3D photonic crystal would represent an extension of the filtered radiator approach (a 1D photonic crystal) with additional dimensions.

The considerable development effort to date of these radiator options has shown the difficulty of achieving the desired spectral emittance performance at high temperatures. Work to date has shown that wavelength selective radiators have spectral efficiencies lower than 50% for low temperature radiators (~1000 ^{o}C). In addition, wavelength selective radiators generally have low above bandgap transmission.

Since wavelength selective radiators inherently operate at high temperatures, the availability of stable materials and configurations with the necessary optical properties is limited. It is important to realize that TPV efficiency and integrated above bandgap transmissivity are proportional to the effective emissivity, which as shown in Eq. (4) couples the hot and cold side emissivity, not the independent emissivity of the two surfaces. As a result, the physical location of spectral improvements on hot or cold side is irrelevant to performance, and any material choice and configuration for a filtered or 3D photonic crystal radiator will be easier to implement on the cold side (TPV cell side) than the hot side (radiator). Not surprisingly, the spectral performance of radiator materials for TPV spectral control lags the performance of front surface tandem filters in an application requiring maximum power density. On the other hand, these radiators may be used in other applications with less stringent power density requirements or applications that can accept a lower power density in exchange for another characteristic offered by these radiating surfaces.

To equal the performance of current front surface tandem filters, selective, filtered, or photonic crystal radiators must achieve a spectral emittance equal to one minus the spectral reflectance of a front surface, tandem filters as shown in Figure 12. This figure shows only the performance at 45° angle of incidence. A radiating surface would need to have high above bandgap emittance with a sharp transition to a low emittance in the below band gap spectral region. In addition, this radiating surface would need to achieve the same performance of the front surface tandem filters at all incidence angles.

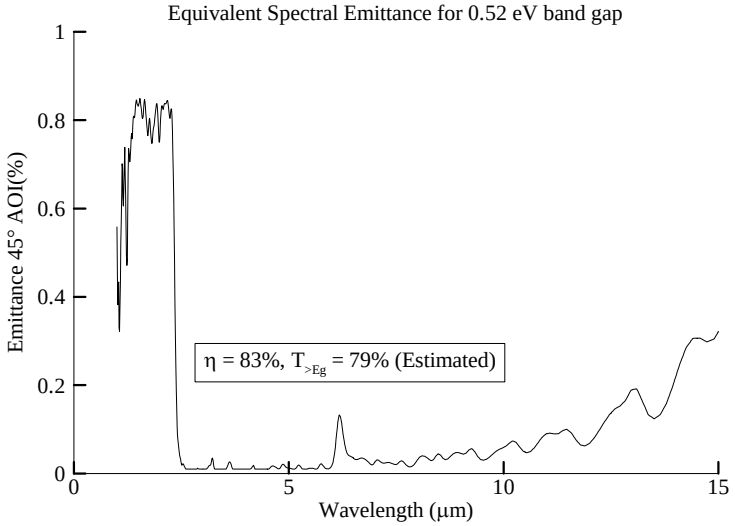

Figure 12 Equivalent Spectral Emittance Needed to Achieve Spectral Performance of Front Surface, Tandem Filters with High Emissivity ($\varepsilon(\lambda,\theta)$~0.8) Radiator.

Conclusions

Our program has focused on front surface filters because, unlike wavelength selective radiators, they operate at lower temperatures. Also, unlike back surface reflectors, front surface filters enable independent optimization of diode performance and spectral control performance (i.e., diode can be designed without regard for long wavelength free carrier absorption). Front surface tandem filters have achieved the highest spectral performance for TPV energy conversion systems. The other, lower performing TPV spectral control options shown in Table 1 may have applications where front surface tandem filters are unsuitable or radiating power needs to be adjusted or controlled (e.g. radioisotope powered TPV systems). The relative performance of each TPV spectral control option is shown in Table 4.

Table 4: Relative Performance of TPV Spectral Control Options

	Spectral Efficiency		
Above Bandgap Transmission	Low	Medium	High
Low	**FSS Filters**		
Medium	**Radiators**		**Tandem Filters**
High		**BSR**	

Various combinations of these spectral control technologies can in some cases be used together to further improve performance. Key technical conclusions include:

- Spectral control performance dominates diode performance in a TPV system and determines the optimum bandgap for a given radiator temperature.
- Low bandgap diodes are conceptually enabling for both higher TPV efficiency and higher power density when spectral control limitations are included.

- Front surface tandem filters have achieved the highest spectral control performance for TPV energy conversion.
- Higher performance for front surface, frequency selective surface (FSS) filters is limited due to finite conductivity of the metal used to create the surface. Therefore, FSS filters do not satisfy the strict requirements for high spectral efficiency and high above band gap transmission as compared to current tandem filter technology
- Back surface reflectors have achieved useful levels of spectral performance but less than the spectral performance of tandem filters. Higher performance for back surface reflectors is limited by free carrier absorption in the diode layers.
- The spectral performance of radiator materials for TPV spectral control lags the performance of front surface, tandem filters for energy conversion in an application requiring maximum power density.

References

1. Siegel and Howell, *Thermal Radiation Heat Transfer*, 3rd edition, (Hemisphere Publishing Corporation, Washington, 1992).
2. C.T. Ballinger, G.W. Charache, C.S. Murray, "Monte-Carlo Analysis of Monolithic Interconnected Module with a Back Surface Reflector," AIP Conf. Proc. **460**, 161 (1999).
3. Baldasaro, P.F., et al., "Thermodynamic Analysis of Thermophotovoltaic Efficiency and Power Density Tradeoffs," Journal of Applied Physics, 2001, **89,** 3319.
4. Wernsman, B., et al., "Greater than 20% Radiant Heat Conversion Efficiency of a Thermophotovoltaic Radiator / Module System Using Reflective Spectral Control," IEEE Transactions on Electron Devices, 2004. **51**(3): p. 512-515.
5. C.K. Gethers, C.T. Ballinger, M.A. Postlethwait, D.M. DePoy, and P.F. Baldasaro, "TPV Efficiency Predictions and Measurements for a Closed Cavity Geometry," AIP Conf. Proc. **401,** 471 (1997).
6. Wanlass, M. W., et al., Proceddings 22nd IEEE Photovoltaic Specialists Conference, pp 38, 1991.
7. Dashiel, et al., 0.52eV Quaternary InGaAsSb Thermophotovoltaic Diode Technology, to be published in proceedings of Sixth Conference on Thermophotovoltaic Generation of Electricity, Freiburg, Germany, 2004.
8. JAP, v. 48, p. 820 (1977)
9. Rahmlow, et al., "New Performance Levels for TPV Front Surface Spectral Control", AIP proceedings of Sixth Conference on Thermophotovoltaic Generation of Electricity, Freiburg, Germany, 2004 (to be published).
10. Fourspring, et al., "Thermophotovoltaic Spectral Control," AIP proceedings of Sixth Conference on Thermophotovoltaic Generation of Electricity, Freiburg, Germany, 2004 (to be published).
11. Fourspring, et al., Optical Coatings for Thermophotovoltaic Spectral Control, Proceedings of OSA Optical Interference Coatings Conference, Tucson, Arizona, 2004 (to be published).
12. DePoy, D.M., et al., "Interference Filters for Thermophotovoltaic Applications," in *Optical Interference Coatings*. 1998, Optical Society of America. p. ThC5-1, ThC5-2.
13. Hickey, C.F., M. Trahan-Verma, and D.M. DePoy, "Antimony Selenide in Multilayer Coatings, in *Optical Interference Coatings*, 2001, Optical Society of America. p. ThE4-1, ThE4-3.
14. Baldasaro, Brown, DePoy, Campbell, Parrington, "Experimental Assessment of Low Temperature Voltaic Energy Conversion," AIP Conf. Proc., **321**, pp 29 (1995).
15. Charache, et al., "Moss-Burstein and Plasma Reflection Characteristics of Heavily-Doped N-type InGaAs and InPAs," J. Appl. Phys. vol **86**, pg 452, 1999.
16. Raynolds, et al., "Theoretical prediction of the plasma frequency and moss-burstein shifts for degenerately doped InAs, InGaAs, and InPAs," AIP Conf. Proc **460**, pg 457 (1998).
17. B. Munk, *Frequency Selective Surfaces*, (John Wiley & Sons, Inc, New York, 2000).
18. T. K. Wu, "Infrared Filters for High Efficiency Thermophotovoltaic Devices," Microwave and Optical Tech. Let. **15**, pp. 9-12 (1997).
19. W. E. Horne, M. D. Morgan, and V. S. Sundaram, "IR Filters for TPV Converter Modules," in *AIP Conf. Proceedings #358,* AIP Conf. Proc. **358**, pg 35 (1995).
20. W. E. Horne and M. D. Morgan, "Filter Array for Modifying Radiant Thermal Energy," U.S. Patent 5,611,870, issued March 18, 1997.
21. E. Topsakal and J. L. Volakis, "On the Properties of Materials for Designing Filters at Optical Frequencies," in Proceedings of the 2003 IEEE AP-S International Symposium and URSI National Radio Science Meeting, 4:635-638, June 2003.
22. J.B. Pryor, "On Ohmic Losses in Frequency Selective Surfaces at Near-Infrared Wavelengths," (Ph.D. Thesis, Ohio State University, Department of Electrical Engineering, 2003, unpublished).
23. Kristensen, Beausang, and DePoy, "Frequency Selective Surfaces as Near Infrared Electro-Magnetic Filters for Thermophotovoltaic Spectral Control ," J. Appl. Phys., **95**, pp. 4845-4851 (2004).
24. Charache, DePoy, Baldasaro, Campbell, "Thermophotovoltaic Devices Utilizing a Back Surface Reflector for Spectral Control," AIP Conf. Proc. **358**, pg 339 (1995).

25. Iles and Chu, “TPV Cells with High BSR,” AIP Conf. Proc. **358**, pg 361 (1995).
26. Clevenger, et al., “Optical Properties of Thin Semiconductor Device Structures with Reflective Back Surface Layers,” AIP Conf. Proc. **460**, pg 327 (1998).
27. Ferguson, L.G. and F. Dogan, A Highly Efficient NiO-Doped MgO Matched Emitter for Thermphotovoltaic Energy Conversion. Materials Science and Engineering B, 2001. **83**: p. 35-41.
28. Ferguson, L.G. and F. Dogan, Spectral Analysis of Transition Metal-Doped MgO "Matched Emitters" for Thermophotovoltaic Energy Conversion. Journal of Materials Science, 2002. **37**: p. 1301-1308.
29. Good, B.S., D.A. Chubb, and A. Pal, Temperature Gradient Effects in an Erbium Aluminum Garnet Selective Emitter, in Thermophotovoltaic Generation of Electricity: Fourth NREL Conference, T.J. Coutts, J.B. Benner, and C.S. Allman, Editors. 1999, The American Institute of Physics: Melville, N.Y. p. 241-248.
30. Heinzel, A., et al., Microstructured Tungsten Surfaces as Selective Emitters, in Thermophotovoltaic Generation of Electricity: Fourth NREL Conference, T.J. Coutts, J.B. Benner, and C.S. Allman, Editors. 1999, The American Institute of Physics: Melville, N.Y. p. 241-248.
31. Pierce, D.E. and G. Guazzoni, High temperature optical properties of thermophotovoltaic emitter components, in Thermophotovoltaic Generation of Electricity: Fourth NREL Conference, T.J. Coutts, J.B. Benner, and C.S. Allman, Editors. 1999, The American Institute of Physics: Melville, N.Y. p. 241-248.
32. Rose, M.F., P. Adair, and K. Schroeder, Selective Emitters for Thermophotovoltaic Power Systems for Use in Aerospace Applications. Journal of Propulsion and Power, 1996. **12**(1): p. 83-88.
33. Sentenac, A. and J.-J. Greffet, Design of Surface Microrelief with Selective Radiative Properties. International Journal of Heat and Mass Transfer, 1994. **37**(4): p. 553-558.
34. Fraas, L., et al., Thermophotovoltaic for Combined Heat and Power Using Low NOx Gas Fired Radiant Tube Burners, in Thermophotovoltaic Generation of Electricity: Fifth Conference, T.J. Coutts, G. Guazzoni, and J. Luther, Editors. 2003, The American Institute of Physics: Melville, N.Y.
35. Crowley, C.J., N.A. Elkouh, and P.J. Magari, *Thermal Spray Approach for TPV Emitters*, in *Thermophotovoltaic Generation of Electricity: Fourth NREL Conference*, T.J. Coutts, J.B. Benner, and C.S. Allman, Editors. 1999, The American Institute of Physics: Melville, N.Y. p. 241-248.
36. Lin, S.-Y., J. Moreno, and J.G. Fleming, *Three-Dimensional Photonic-Crystal Emitter for Thermo Photovoltaic Power Generation.* Applied Physics Letters, 2003. **83**(2): p. 380-382.